Improved Discrete Random Walk Stochastic Model for Simulating Particle Dispersion and Deposition in Inhomogeneous Turbulent Flows

Amir A. Mofakham
Department of Mechanical and Aeronautical Engineering,
Clarkson University,
Potsdam, NY 13699-5725
e-mail: abdolla@clarkson.edu

Goodarz Ahmadi
Department of Mechanical and Aeronautical Engineering,
Clarkson University,
Potsdam, NY 13699-5725
e-mail: gahmadi@clarkson.edu

The performance of different versions of the discrete random walk models in turbulent flows with nonuniform normal root-mean-square (RMS) velocity fluctuations and turbulence time scales were carefully investigated. The OpenFOAM $v^2 - f$ low Reynolds number turbulence model was used for evaluating the fully developed streamwise velocity and the wall-normal RMS velocity fluctuations profiles in a turbulent channel flow. The results were then used in an in-house MATLAB particle tracking code, including the drag and Brownian forces, and the trajectories of randomly injected point-particles with diameters ranging from 10 nm to 30 μm were evaluated under the one-way coupling assumption. The distributions and deposition velocities of fluid-tracer and finite-size particles were evaluated using the conventional-discrete random walk (DRW) model, the modified-DRW model including the velocity gradient drift correction, and the new improved-DRW model including the velocity and time gradient drift terms. It was shown that the conventional-DRW model leads to superfluous migration of fluid-point particles toward the wall and erroneous particle deposition rate. The concentration profiles of tracer particles obtained by using the modified-DRW model still are not uniform. However, it was shown that the new improved-DRW model with the velocity and time scale drift corrections leads to uniform distributions for fluid-point particles and reasonable concentration profiles for finite-size heavy particles. In addition, good agreement was found between the estimated deposition velocities of different size particles by the new improved-DRW model with the available data. [DOI: 10.1115/1.4047538]

Keywords: discrete random walk (DRW) model, stochastic model, deposition velocity, concentration profiles, OpenFOAM, $v^2 - f$ low Reynolds turbulence model

1 Introduction

An accurate model for estimating the deposition and distribution of micro- and nanoparticles in turbulent flows is of vital interest to a wide range of industrial [1], environmental [2], and biomedical processes [3–7]. For simulating these processes, accurate simulation of the turbulent flow field is needed. Currently, there are three main approaches for simulating turbulent flows. In the direct numerical simulation (DNS), all scales of turbulence up to the Kolmogorov scale are resolved. While the DNS approach is the most accurate method, it requires extensive computational resources. At present, the applications of DNS have been limited to simple flow passages for fundamental research studies, and the prohibitive computational cost has made the DNS approach inapplicable to industrial applications. Large eddy simulation (LES) is another approach that resolves the details of turbulent flows larger than the grid cell size, and only the subgrid-scale fluctuations are modeled where a dispersion model also needs to be used to include the effects of small scale turbulent eddies on particle motions [8,9]. While the LES requires less computational resources compared to the DNS, it is still computationally demanding for simulating flows in complex passages at high Reynolds numbers. The approach that is more commonly used for industrial applications is the Reynolds-averaged Navier–Stokes (RANS) model. While quite economical, the RANS model evaluates only the time-averaged velocities and turbulence statistics (root-mean-square (RMS) turbulence fluctuations). Therefore, for particle trajectory analysis and accounting for turbulence dispersion effects in turbulent particle-laden flows, the instantaneous fluctuations must be modeled. The discrete random walk (DRW) and continuous random walk (CRW) models are the most commonly used approaches which were originally suggested for homogenous turbulent flows [10,11]. Later, it was found that using the conventional stochastic models in turbulent flows with inhomogeneous turbulent velocity scale leads to unrealistic particle dispersion, so extensive studies were conducted to improve the performance of turbulence stochastic models in inhomogeneous turbulent flows [12–20]. In these investigations, different corrections were suggested to mitigate the effects of the mean-square fluctuation velocity inhomogeneities. However, the inhomogeneities of the turbulence time scale can also affect the performance of the stochastic models [21–24]. Recently, Mofakham and Ahmadi [19] showed that the Normalized-CRW model (in the absence of the time correction) results in accurate particle dispersions and depositions in a turbulent channel flow with inhomogeneous turbulence time scale. Therefore, it is concluded that the inhomogeneities of the turbulence time scale do not adversely affect the performance of the CRW model.

The performance of various CRW models were already discussed by Mofakham and Ahmadi [19] and the normalized-CRW model was suggested as the most accurate CRW model. Later, the normalized-CRW was implemented into the ANSYS-FLUENT code to improve its predictions of particle dispersions and depositions in inhomogeneous turbulent flows [20]. However, a detailed study

Contributed by the Fluids Engineering Division of ASME for publication in the JOURNAL OF FLUIDS ENGINEERING. Manuscript received March 24, 2020; final manuscript received June 4, 2020; published online July 13, 2020. Assoc. Editor: Arindam Banerjee.

on the performance of the DRW model in inhomogeneous flows has not been conducted in the past. The present study is focused on exploring the performance of the DRW model, which is commonly used in commercial software, in a turbulent channel flow. The aim of this investigation is to clarify the effects of the inhomogeneities of the turbulence velocity and time scales on the performance of different versions of the DRW model and also to develop the most accurate DRW model for predicting the dispersion and deposition of micro- and nanoparticles in inhomogeneous turbulent flows.

The time-averaged fluid velocities and mean-square fluctuation velocities in a two-dimensional fully developed turbulent duct flow were first evaluated by the v^2-f model of the OpenFOAM CFD software. The results were then used to generate the instantaneous velocity fluctuations, as seen by fluid-tracer and finite-size particles using three different versions of the DRW model. The first model was the conventional-DRW model (in the absence of drift corrections), which was originally developed by Gosman and Ioannides [11] for homogenous turbulent flows. It was shown that the conventional-DRW model leads to superfluous migration of fluid-point particles toward the wall and an erroneous particle deposition rate. Then, the modified-DRW model proposed by Bocksell and Loth [15] with an appropriate velocity gradient drift correction term was tested. It was found that the predicted concentration profiles of tracer particles, while improved, still are not uniform. It was hypothesized that the reason for this discrepancy is the inhomogeneous turbulence time macroscale in the channel flow. A new drift correction term as a function of gradients of both RMS fluctuation velocity and the turbulence time macroscale was proposed. It was shown that the new improved-DRW model with the velocity and time scale drift corrections leads to uniform distributions of fluid-point particles and reasonable concentration profiles for finite-size particles. The new improved-DRW model was used, and the deposition velocities of different size particles were evaluated. Good agreement was found between the simulated deposition velocities with the available experimental data, as well as the predictions of the empirical models and earlier DNS results.

2 Methods

2.1 Computational Domain. It is assumed that air with a kinematic viscosity of $1.46\times10^{-5}\,\mathrm{m^2/s}$ at a temperature of 293 K and a mean velocity of 5 m/s flows in a two-dimensional channel. The corresponding flow Reynolds number based on the half-height of the channel is 3423 for which a shear velocity of 0.32 m/s is estimated by the Colebrook–White empirical equation. In this study, u^*, ν/u^*, and, ν/u^{*2} are, respectively, the characteristic velocity, length, and time scales for nondimensionalizing all parameters. Accordingly, the nondimensional length, L^+, and half-width, H^+, of the channel are, respectively, 1095 and 219 wall units. The geometry of the channel and the grid were generated by the mesh generation utility, blockMesh, provided by OpenFOAM. The domain in the streamwise direction is uniformly discretized by 100 nodes. However, in order to capture the steep variations of parameters along the wall-normal direction near the wall, it is essential to have sufficiently refined grids in the wall-normal direction. In this regard, the domain is discretized with 100 nodes in the wall-normal direction, where a boundary layer grid is constructed for the near-wall regions providing smaller grids adjacent to the wall and larger grids in the core region.

2.2 Flow Simulation. Accurate estimation of the wall-normal RMS velocity fluctuations near the wall is essential for obtaining accurate results for the deposition rate of micro- and nanoparticle [19,20,25]. However, many RANS turbulence models overestimate the near-wall normal RMS values. Among the available turbulence models, the v^2-f (or $k-\varepsilon-\overline{v^2}$) model which was originally proposed by Durbin [26,27] appears to predict the quadratic variation of the normal RMS velocity fluctuations in the near-wall regions with reasonable accuracy without using an ad hoc near-wall viscous damping function. The correct wall blocking effects were incorporated by employing the mean-square wall-normal velocity fluctuations, $\overline{v'^2}$, instead of the turbulence kinetic energy to evaluate the eddy viscosity (Eq. (3)) and employing an elliptic-relaxation equation [26,27]. In this investigation, the turbulent channel flow is simulated using the v^2-f turbulence model of the OpenFOAM CFD package [28,29] where the standard k–ε modle equations are solved for evaluing the turbulence kinetic energy and the disspation rate. That is

$$\frac{\partial k}{\partial t}+u_i\frac{\partial k}{\partial x_i}=P_{\mathrm{k}}-\varepsilon+\frac{\partial}{\partial x_j}\left[\left(\nu+\frac{\nu_t}{\sigma_k}\right)\frac{\partial k}{\partial x_j}\right] \tag{1}$$

$$\frac{\partial \varepsilon}{\partial t}+u_i\frac{\partial \varepsilon}{\partial x_i}=\frac{C_{\varepsilon_1}P_k-C_{\varepsilon_2}\varepsilon}{\mathrm{T_t}}+\frac{\partial}{\partial x_j}\left[\left(\nu+\frac{\nu_t}{\sigma_\varepsilon}\right)\frac{\partial \varepsilon}{\partial x_j}\right] \tag{2}$$

where ν is the kinematic viscosity, ν_t is the eddy-viscosity given by

$$\nu_t=C_\mu\overline{v'^2}T_t. \tag{3}$$

In Eqs. (1) and (2), the turbulence production term, P_k is defined as

$$P_k=\nu_t\frac{\partial u_i}{\partial x_j}\left(\frac{\partial u_i}{\partial x_j}+\frac{\partial u_j}{\partial x_i}\right) \tag{4}$$

and the Eulerian turbulence time scale T_t is defined by

$$T_t=\max\left[\frac{k}{\varepsilon},6\sqrt{\frac{\nu}{\varepsilon}}\right] \tag{5}$$

The evolution of the mean-square wall-normal velocity fluctuations, $\overline{v'^2}$, and the elliptic relaxation function, f, are governed by

$$\frac{\partial u_i\overline{v'^2}}{\partial x_j}=\frac{\partial}{\partial x_j}\left[(\nu+\nu_t)\frac{\partial \overline{v'^2}}{\partial x_j}\right]+kf-6\overline{v'^2}\frac{\varepsilon}{\mathrm{k}} \tag{6}$$

$$L_t^2\frac{\partial^2 f}{\partial x_i^2}-f-\frac{1}{T_t}\left[(C_1-6)\frac{\overline{v'^2}}{k}-\frac{2}{3}(C_1-1)\right]+C_2\frac{P_k}{k}=0 \tag{7}$$

where the turbulence length scale L_t is defined as

$$L_t=\mathrm{C_L}\max\left[\frac{k^{3/2}}{\varepsilon},c_\eta\left(\frac{\nu^3}{\varepsilon}\right)^{1/4}\right] \tag{8}$$

In this study, the Reynolds-averaged Navier–Stokes equations and Eqs. (1)–(8) are solved by the pisoFoam solvers of the OpenFOAM software with the empirical coefficients listed in

Table 1 The default empirical coefficients of the OpenFOAM v^2-f turbulence model

C_μ	0.22
C_1	1.4
C_2	0.3
C_L	0.23
C_η	70
C_{ε_1}	$1.4\left(1+0.050\left(k/\overline{v'^2}\right)^{0.5}\right)$
C_{ε_2}	1.9
σ_k	1
σ_ε	1.3

Table 2 The boundary conditions of different variables imposed on the walls (values are in wall units)

ε	Fixed value (0.2)
f	0
k	0
ν_t	Zero gradient
p	Zero gradient
$\mathbf{u}$	(0 0 0)
$\overline{v'^2}$	0

Table 3 The growth factors and the wall distance of the first grid points in wall units of different grids

	Growth factor	First grid point wall distance
Grid 1	1	4.38
Grid 2	10	1.11
Grid 3	35	0.45
Grid 4	70	0.26
Grid 5	200	0.11

Table 1 and the wall boundary conditions listed in Table 2. To reach a fully developed flow, the simulations are carried out with a cyclic boundary condition for all variables at the inlet and outlet, while the fvOptions framework of OpenFOAM that adds a force in the momentum equation is used to maintain a mean streamwise velocity with a nondimensional value of 15.6 wall units.

To make sure that the near-wall grid sizes are sufficiently small, computational grids with 100 nodes in the x- and y-directions are constructed with various growth factors listed in Table 3, which results in grids with different near-wall grid sizes. The corresponding wall-normal fluid velocity fluctuations predicted by the v^2-f model, whose accuracy is critical for getting reasonable particle distributions and deposition velocities, are evaluated and plotted in Fig. 1. To clarify the accuracy of the near-wall predictions of the v^2-f model, the results are compared with those of the ANSYS-FLUENT Reynolds stress transport model (RSTM) in conjunction with the enhanced wall function for a turbulent duct flow with shear Reynolds number of 219 [19,20], the near-wall

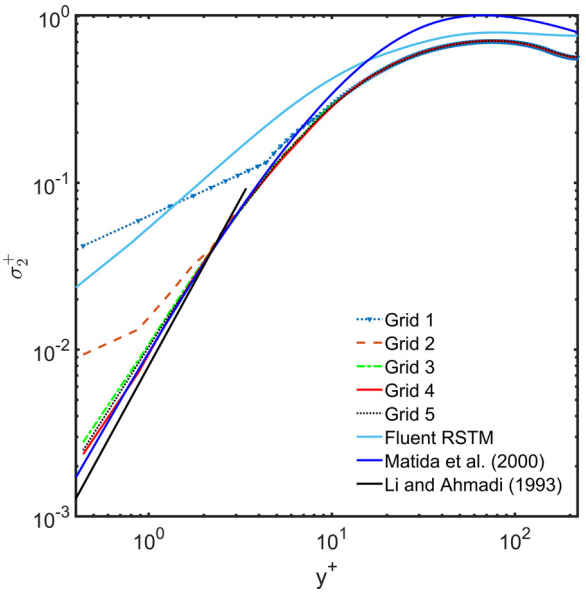

Fig. 1 The comparison of the predictions of the wall-normal velocity fluctuations by the OpenFOAM v^2-f model for the grids listed in Table 3 with those of the ANSYS-FLUENT RSTM model and the empirical models are given by Eqs. (9) and (10).

estimations of the empirical model suggested by Ounis et al. [30], and Li and Ahmadi [31] for $y^+ < 4$

$$\sigma_2^+ = A\, y^{+2} \tag{9}$$

where $A = 0.008$ [25], and the predictions of the empirical model proposed by Matida et al. [32] obtained from the DNS data which is given by

$$\sigma_2^+ = \frac{0.0116 y^{+2}}{1 + 0.203 y^+ + 0.0014 y^{+2.421}} \tag{10}$$

Figure 1 illustrates the v^2-f model overestimates the wall-normal velocity fluctuations for grids 1 and 2 that have relatively large cell sizes near the wall. However, the predictions of grids 3–5 are in good agreement with the empirical models given by Eqs. (9) and (10). This confirms that the v^2-f model correctly estimates the near-wall quadratic variation of the wall-normal velocity fluctuations if the near-wall regions are gridded with sufficiently small cells. Since the predictions for grids 3–5 are almost identical, grid 3 is used in the present study. It is also concluded that the results obtained with the use of grid 3 are independent of the near-wall grid sizes. Figure 1 also shows the inability of the ANSYS-FLUENT RSTM model in accurately predicting the near-wall values of the wall-normal velocity fluctuations despite using the enhanced wall function, as was discussed earlier [19,25].

2.3 Lagrangian Particle Tracking Model. For particle transport analysis, at least 2×10^5 point particles with a density ratio (ratio of particle density to that of the fluid) $S = 2000$ are randomly introduced in the channel, and their trajectories were evaluated. The equation of motion of a spherical particle in the absence of gravity and lift forces is given by

$$\frac{du_i^p}{dt} = \frac{1}{\tau_p}\frac{C_D \mathrm{Re}_\mathrm{p}}{24}\left(u_i - u_i^p\right) + n_i(t) \tag{11}$$

where u_i^p is the ith component of particle velocity, u_i is the ith component of fluid velocity, and τ_p is the particle relaxation time given as

$$\tau_p = \frac{S d_p^2 C_c}{18\nu} \tag{12}$$

where S is the density ratio, d_p is the particle diameter, and C_c is the Cunningham slip correction factor given as

$$C_c = 1 + \frac{2\lambda}{\mathrm{d_p}}\left(1.257 + 0.4\mathrm{e}^{-\frac{1.1\mathrm{d_p}}{2\lambda}}\right) \tag{13}$$

where λ is the gas mean free path which is picked equal to 7×10^{-8} (m) for air in the current study.

In Eq. (11), $\mathrm{Re_p} = d_p|\mathbf{u} - \mathbf{u}_p|/\nu$ is the particle Reynolds number, and $\mathrm{C_D}$ is the drag coefficient which is given by [33]

$$C_D = \frac{24}{\mathrm{Re_p}}\left(1 + 0.15\mathrm{Re_p}^{0.687}\right) \tag{14}$$

The Brownian force is modeled as a Gaussian white noise random process [31]. Accordingly, at each time-step, the amplitude of the Brownian force per unit mass is given as

$$n_i(t) = G(t)\left(\frac{\pi S_0}{\Delta t}\right)^{0.5} \tag{15}$$

where $G(t)$ is a zero mean, unit variance Gaussian random number, Δt is the time step used, and the spectral intensity of the noise, S_0, is given by

$$S_0 = \frac{2k_bT}{\tau_p \pi m} \tag{16}$$

where $k_b = 1.38 \times 10^{-23}$ J/K is the Boltzmann constant, T is the absolute temperature (K), and m is the mass of the particle.

2.4 Deposition Velocity. For particles, a trap boundary condition on the lower and upper walls is used. That is, if a particle distance to one of the walls is less than its radius, the particle is assumed to be deposited on the wall. Then, the particle is added to the accumulative number of deposited particles on the walls, and is not tracked anymore. To keep the number of particles constant during the simulations, when a particle is deposited, another particle is randomly introduced in the channel. For the streamwise direction, a periodic boundary condition is imposed, which means if a particle passes the outlet of the channel, it is reinjected from the inlet with the same velocities and normal distance from the wall.

For assessing the performance of the DRW models, numbers of deposited particles with different diameters on the walls are recorded in time for all simulations, and the results are used in the following equation to evaluate the nondimensional deposition velocity:

$$u_d^+ = \frac{N_0 H^+}{N_p t_d^+} \tag{17}$$

where N_0 and N_p are, respectively, the total number of particles and the number of deposited particles in the time interval of t_d^+. The resulting deposition velocities are then compared with the experimental data, earlier numerical results, the DNS data, as well as the empirical models of Fan and Ahmadi [34] and Wood [35]. The empirical equation of Fan and Ahmadi [34] in the absence of gravity and wall roughness is given as

$$u_d^+ = \begin{cases} 0.084\, Sc^{-\frac{2}{3}} + \left[\dfrac{d_p^+}{5.23}\right]^{2/(1+\tau_p^+ 2L_1^+)} & \text{if } u_d^+ \le 0.14, \\ 0.14 & \text{otherwise} \end{cases} \tag{18}$$

where $L_1^+ = 3.08/(Sd_p^+)$.

The empirical equation of Wood [35] is given as

$$u_d^+ = 0.057\, \mathrm{Sc}^{-2/3} + 4.5 \times 10^{-4} \tau_p^{+2} \tag{19}$$

where τ_p^+ is the nondimensional particle relaxation time, $\mathrm{Sc} = \nu/D$ is the Schmidt number with D being the particle mass diffusivity given as

$$D = \frac{k_bT}{3\pi\mu d_p} C_c \tag{20}$$

2.5 Turbulence Dispersion Models. For incorporating the effects of turbulence velocity fluctuations on particle dispersions and depositions, three different DRW models are used. In addition to the DRW models, the normalized-CRW model that was shown to be able to predict reasonable results in inhomogeneous turbulent flows [19] is also used, and its results are compared with those of the DRW models to assess the relative performance of the DRW models to the normalized-CRW model.

2.5.1 Conventional-Discrete Random Walk Model. According to the Conventional-DRW stochastic model, the instantaneous velocity fluctuations seen by a particle in the i-direction is given by

$$u_i'^{n+1} = \sigma_i G_i \tag{21}$$

where G_i is selected from a population of independent Gaussian random numbers with zero mean and unit variance, and σ_i is the RMS turbulence velocity fluctuations obtained from the RANS simulation. As noted before the $v^2 - f$ turbulence model provides the variance of wall-normal velocity fluctuations, $\overline{v'^2}$ and the turbulence kinetic energy, but it does not evaluate the variance of streamwise velocity fluctuations. The RMS velocity fluctuations in the y-direction in a channel, σ_2, is equal to the square root of the variance of the wall-normal velocity fluctuations, ($\sigma_2 = \sqrt{\overline{v'^2}}$). Although the streamwise velocity fluctuations can be approximately estimated from the wall-normal RMS velocity fluctuations and the turbulence kinetic energy [36], the streamwise velocity fluctuations are ignored in this investigation. This is because the streamwise velocity fluctuations do not affect the particle distributions and depositions in a straight channel with smooth walls, and the stochastic models are only used to generate the wall-normal velocity fluctuations.

During the tracking of a particle, σ_i is updated based on the particle location while a new random number G_i is generated after the eddy interaction time (t_{int}). Brown and Hutchinson [37] and Gosman and Ioannides [11] proposed the following expression for the eddy interaction time interval:

$$t_{\mathrm{int}} = \min(\tau_e, t_R) \tag{22}$$

where t_R is the eddy transit time which is the time a particle needs to cross an eddy as a result of its slip velocity, which is given by

$$t_R = -\tau_p \ln\left[1 - \left(\frac{L_e}{\tau_p |\mathbf{u} - \mathbf{u}^p|}\right)\right] \tag{23}$$

In Eq. (22), τ_e is the eddy lifetime for which different expressions were proposed in the literature [13]. In this investigation, it was assumed $\tau_e = 2T_L$ where the Lagrangian integral time scale, T_L, is evaluated by the expressions of Kallio and Reeks [38] given as

$$T_L^+ = T_L u^{*2}/\nu = \begin{cases} 10 \text{ if } y^+ \le 5 \\ 7.122 + 0.5731 y^+ - 0.00129 y^{+2} \text{ if } 5 < y^+ < 200 \end{cases} \tag{24}$$

Although these expressions were proposed for $0 < y^+ < 200$, in this investigation, they were used across the channel with half-height of 219 wall units.

Similar to σ_i, during the tracking of a particle, τ_e is updated based on the particle location at each time-step.

2.5.2 Modified-Discrete Random Walk Model. It is known that the conventional-DRW model leads to an unrealistic accumulation of fluid-tracer particles in the near-wall regions of inhomogeneous turbulent flows [13,15]. To rectify this issue, Eq. (21) was modified by the researchers to the following equation:

$$u_i'^{n+1} = \sigma_i G_i + \overline{u_i'^{n+1}} \tag{25}$$

where the second term on the right-hand side of the equation is a mean drift velocity correction term that is a function of the turbulence velocity gradient and is added to improve the predictions of particle distributions in inhomogeneous turbulent flows. While different expressions for the drift terms of the DRW model were suggested in the literature, in the present study the drift term suggested by Bocksell and Loth [15] and the finite-inertia drift coefficient ($1/(1 + \mathrm{St}k)$) recommended by Bocksell and Loth [39] are used. Accordingly, the expression for the mean drift correction term of the modified-DRW model is given as

$$\overline{u_i'^{n+1}} = \overline{u_i'^{n}} + \frac{1}{1 + \mathrm{Stk}} \sigma_i \frac{\partial \sigma_i}{\partial x_j} \Delta t \tag{26}$$

where $\mathrm{Stk} = \tau_p/T_L$ is the Stokes number. The coefficient $1/(1 + \mathrm{Stk})$ is the finite-inertia drift coefficient that accounts for the

particle and fluid decorrelation. Based on Eq. (26), during the lifetime of an eddy, the drift term is summed over the time steps until the particle residence time reaches the eddy lifetime, then the random number G_i is updated and a new drift term is evaluated.

2.5.3 Improved-Discrete Random Walk Model. The presently proposed improved-DRW model is similar to the modified-DRW model, except a drift term as a function of the gradient of the Lagrangian time scale is also added to the velocity gradient drift term. Accordingly, Eq. (26) is replaced by the following equation:

$$\overline{u_i'^{n+1}} = \overline{u_i'^{n}} + \frac{1}{1+\mathrm{Stk}}\left(\sigma_i \frac{\partial \sigma_i}{\partial x_j} - \frac{\sigma_i^2}{T_L}\frac{\partial T_L}{\partial x_j}\right)\Delta t \tag{27}$$

The inclusion of the gradient of the Lagrangian integral time scale in the drift term was first suggested by Monin and Yaglom [21] in their formulation of the Fokker–Planck equation model for inhomogeneous turbulent flows. Hence, in this investigation, a correction term as a function of the time gradient term is included to mitigate the effects of time-scale inhomogeneities on the prediction of DRW particle distributions.

Similar to the modified-DRW model, during the lifetime of an eddy, the corresponding drift term is added over the time-step until the eddy lifetime is reached. Then, a new random number G_i is selected, and the new drift term is evaluated.

2.5.4 Normalized-Continuous Random Walk Model. The normalized-CRW model is concluded from the normalized Langevin equation given as

$$\frac{d}{dt}\left(\frac{u_i'}{\sigma_i}\right) = -\frac{u_i'}{\sigma_i T_L} + \sqrt{\frac{2}{T_L}}\xi_i + A_i \tag{28}$$

where ξ_i is a Gaussian white noise process with a zero mean, and an autocorrelation function that is a Dirac delta function, and A_i is the drift correction term, which needs to be included in inhomogeneous turbulent flows to get reasonable results. For a channel flow, A_i in the x- and y-direction is given as [40]

$$A_1 = \frac{1}{1+\mathrm{Stk}}\frac{\partial\overline{\left(\frac{u_1'u_2'}{\sigma_2}\right)}}{\partial x_2} \tag{29}$$

$$A_2 = \frac{1}{1+\mathrm{Stk}}\frac{\partial \sigma_2}{\partial x_2} \tag{30}$$

Integrating Eq. (28) results in the following Markov chain relationship:

$$u_i'^{n+1} = \frac{\sigma_i^{n+1}}{\sigma_i^n}u_i'^{n}\exp\left(-\frac{\Delta t}{\tau_i}\right) + \sigma_i^{n+1}\left(1-\exp\left(-2\frac{\Delta t}{\tau_i}\right)\right)^{\frac{1}{2}}G_i + \sigma_i^{n+1}\tau_i A_i^{n+1}\left(1-\exp\left(-\frac{\Delta t}{\tau_i}\right)\right) \tag{31}$$

Additional details of the CRW model are described by Mofakham and Ahmadi [18–20].

3 Results and Discussion

In this section, first, the predictions of the v^2-f turbulence model for the fluid time-averaged velocities and turbulence statistics are presented. Then, the results are used to generate the instantaneous velocity fluctuations in turbulent channel flows by the conventional-, modified-, and improved-DRW models. The performances of these DRW models are examined by exploring their predictions of fluid-tracer and finite-size particle concentration distributions. Their predictions of different DRW models for micro- and nanoparticle deposition velocities are also evaluated, and the results are compared with the available experimental data and numerical results.

3.1 Fluid Flow Simulation. The mean flow streamwise velocity, the wall-normal RMS fluid velocity fluctuations, the turbulence kinetic energy, and the turbulence dissipation rate predicted by the v^2-f turbulence model of the OpenFOAM CFD software are plotted in Fig. 2 versus the wall distance to the lower wall in wall units (y^+). To assess the accuracy of these results, they are compared with the predictions of the ANSYS-FLUENT RSTM turbulence model for a duct flow with shear Reynolds number of 219 [19,20] and the available DNS channel data.

The streamwise mean velocity profile predicted by the v^2-f model is plotted in Fig. 2(*a*) and compared with the near-wall log-law profile, the DNS channel data at shear Reynolds number of 219 resulted by the pseudo-spectral code [41–44], which are labeled as DNS, and the DNS results of Kim et al. [45]. Although the comparison illustrates that the RSTM turbulence model predicts a more accurate estimation of the streamwise velocity profile, the prediction of the v^2-f model is also in a good agreement with the DNS data and the near-wall log-law profile.

The wall-normal RMS fluid velocity fluctuation and the turbulence kinetic energy predictions of the v^2-f model are, respectively, plotted in Figs. 2(*b*) and 2(*c*) and compared with the DNS results at the shear Reynolds number of 219, the DNS reported by Kim et al. [45] and Moser et al. [46] for the shear Reynolds number of 180, and the estimations of the RSTM model. The comparison in Fig. 2(*b*) reveals that the v^2-f turbulence model predictions of the wall-normal RMS velocity fluctuation has a similar trend as the DNS results but underestimates its magnitude. Figure 2(*c*) confirms a good agreement between the turbulence kinetic energy predictions of the v^2-f model in the core region, but show small discrepancies in the near-wall region in comparison to the DNS results with shear Reynolds number of 219.

Figure 2(*d*) illustrates the turbulence dissipation rate as predicted by the v^2-f turbulence model and the DNS results with shear Reynolds number of 219, the DNS results of Mansour et al. [47] for the shear Reynolds number of 180, and the RSTM model estimations. This figure shows a good agreement between the predictions of the v^2-f model and the DNS data in the core region, while the dissipation rates are underestimated in the near-wall regions.

From the comparison of the predictions of the v^2-f model with those of the RSTM model in Fig. 2, it appears that the v^2-f model predicts the turbulence kinetic energy and the turbulence dissipation rate more accurately, while the RSTM mean streamwise velocity predictions are in a better agreement with the log-law velocity profile. There are some discrepancies for predictions of the wall-normal velocity fluctuation of both the v^2-f model and the RSTM model with the DNS results, but it seems that the estimations of the RSTM model are somewhat closer to the DNS data. However, as it was discussed in Fig. 1, the v^2-f model more accurately predicts the RMS wall-normal velocity fluctuation profile at the near-wall regions which is critical for getting accurate deposition velocities which makes the v^2-f more appropriate for the present study.

3.2 Fluid-Tracer Particles. It is known that a homogenous distribution of fluid-tracer particles should stay uniform in homogenous or inhomogeneous turbulent flows. Therefore, by exploring the fluid-tracer particle concentration profiles predicted by different DRW models, the performance of these models can be examined. Here, the influences of including or ignoring the velocity and the time scale gradient terms on the results are studied.

The normalized concentration profiles and the particle distributions of fluid-tracer particles after 10,000 wall units obtained by the conventional-DRW model, Eq. (25) are shown in Fig. 3. Figure 3(*a*) shows the time evolutions of the normalized

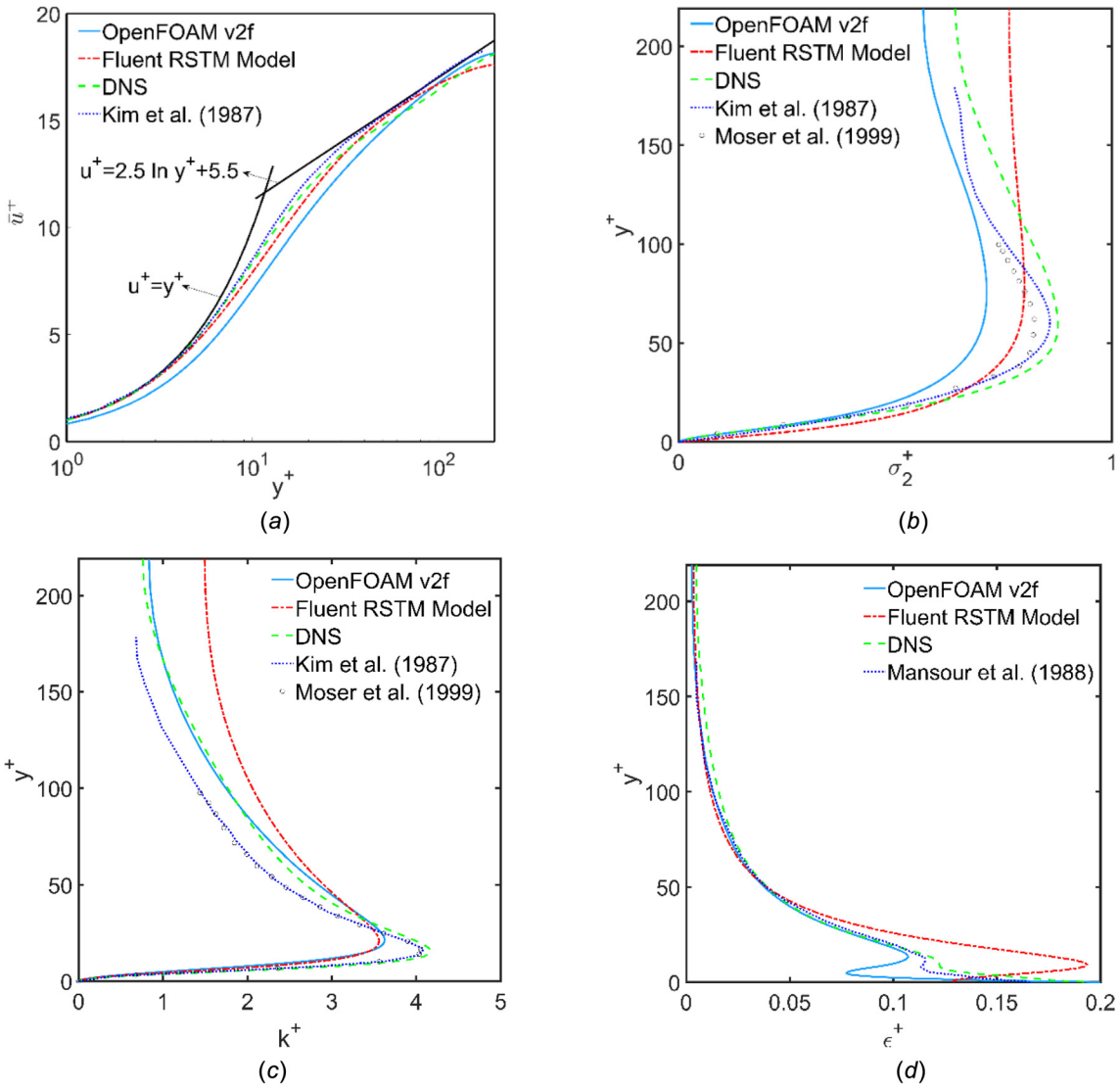

Fig. 2 Comparisons of different profiles with DNS results and the RSTM model: (*a*) mean streamwise fluid velocity profile, (*b*) RMS normal fluid velocity fluctuations profile, (*c*) turbulence kinetic energy pofile, and (*d*) turbulence dissipation rate profile

concentration profiles up to a time duration of 10,000 wall units in the lower half of the channel versus $\eta = y/H$. Here, y is the distance from the wall, and H is the half height of the channel. This figure shows that the concentration profile of fluid-tracer particles almost reaches the steady-state condition. However, the concentration is inhomogeneous rather with large values at the walls. That is, using the conventional-DRW model leads to a normalized concentration of 1.3 in the core region and a rather sizeable value of 244 at the wall. The corresponding particle distributions at 10,000 wall units are also shown in Fig. 3(*b*). In this figure, $\chi = x/H$, where x is the x-axis, and H is the half height of the channel. This figure confirms the nonuniform distributions of fluid-tracer particles predicted by the conventional-DRW model.

For improving the performance of the conventional-DRW model, the modified-DRW model given by Eq. (25) is used. The modified-DRW model includes the drift correction described by Eq. (26) that is proportional to the gradient of the RMS normal velocity fluctuations. Figure 4(*a*) shows the time evolutions of fluid-tracer particle concentration profiles up to a duration of 10,000 wall units as predicted by the modified-DRW model. This figure shows that using the modified model leads to a steady-state concentration profile but is still nonuniform. The high normalized concentration of fluid-tracer particles predicted by this model is about 1.4 in the core region, and the low concentration is around 0.2 in the near-wall regions. The particle distribution at 10,000 wall units is depicted in Fig. 4(*b*), which confirms the higher concentration of particles in the core region and the low concentration in the near-wall region.

Since the modified-DRW model is not able to correctly predict a uniform distribution for fluid-tracer particles, it was suspected that the concentration of particles is affected by the inhomogeneity of the turbulence time-scale. For examining this hypothesis, the modified-DRW model with an inhomogeneous RMS velocity fluctuation but with a homogenous time scale is studied. The corresponding simulation results showed a uniform tracer particle distribution. These results, however, are not reported here for the sake of brevity.

For rectifying this issue, based on the Fokker–Planck equation suggested by Monin and Yaglom [21], a new drift term as a function of the gradient of Lagrangian time scale was included in the mean drift term of the improved-DRW model as given by Eq. (27). As was noted by Durbin [22], in turbulent flows with an inhomogeneous Lagrangian time scale, the particle motion tends to persist longer in the direction of increasing time scale, which leads to the migration of particles toward the regions with larger time scales. It should be emphasized that particles migrate from

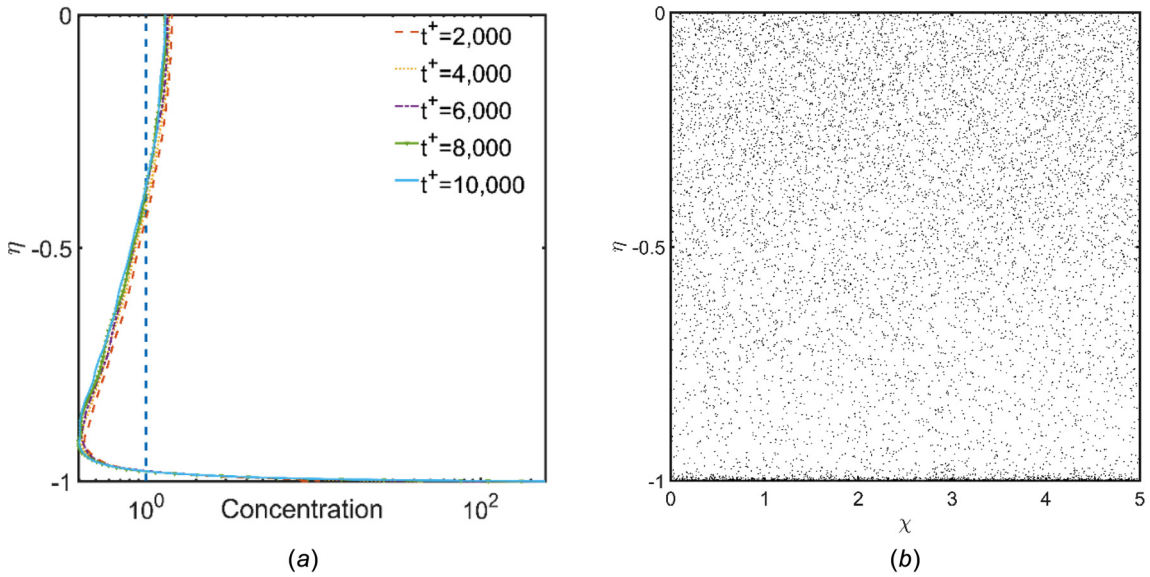

Fig. 3 (*a*) Time evolutions of fluid-tracer normalized concentration profiles and (*b*) particle distributions at 10,000 wall units as predicted by the conventional-DRW model

regions with larger velocity fluctuation toward the regions with lower velocity fluctuation (if the velocity gradient drift term is ignored). These explain why the velocity gradient drift term has a positive sign, while the drift term as a function of time gradient has a negative sign in Eq. (27).

Using the improved-DRW with both velocity and time gradients drift terms leads to the fluid-tracer particle concentration profiles and distributions shown in Fig. 5. Figure 5(*a*) shows that the improved-DRW model predicts steady and roughly uniform concentration profiles for fluid-tracer particles, with a small accumulation and depletion of particles in the near-wall region. Figure 5(*b*) also confirms that employing the improved-DRW results in uniform distributions of fluid-tracer particles at 10,000 wall units. The results presented in Fig. 5 verifies that the improved-DRW model is effective in predicting the correct fluid-tracer concentration profiles in turbulent flows with inhomogeneous fluctuation velocity and Lagrangian time scale.

The concentration profiles of fluid-tracer particles predicted by the conventional-, modified-, improved-DRW models, and the normalized-CRW model (Eq. (31)) [19] are plotted in Fig. 6 for comparison. To provide a better understanding of the differences between the predictions of different versions of the DRW model, the variations along the lower half-height of the channel are presented in a linear plot in Fig. 6(*a*), and the near-wall variations are also presented in a log–log plot versus y^+in Fig. 6(*b*). It is seen that the conventional-DRW model predicts an unrealistic large concentration in the near-wall region. While using the modified-DRW model leads to a significant reduction of the near-wall accumulation of particles, the predicted concertation profile is still inhomogeneous. The newly proposed Improved-DRW similar to the normalized-CRW model predicts an almost uniform normalized concentration of about 1, which confirms the advantage of the proposed Improved-DRW model.

3.3 Finite-Inertia Coefficient. In Sec. 3.2, it was concluded that the improved-DRW model is able to predict a uniform distribution for fluid-tracer particles with reasonable accuracy. In this section, the predictions of the improved-DRW model for finite-size particle distributions are investigated.

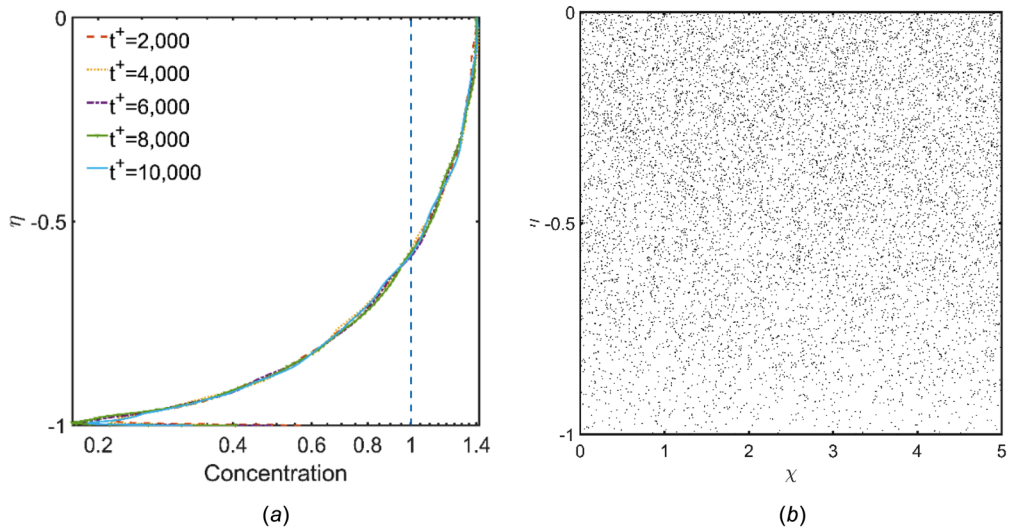

Fig. 4 (*a*) Time evolutions of fluid-tracer normalized concentration profiles, and (*b*) particle distributions at 10,000 wall units when the modified-DRW model is used

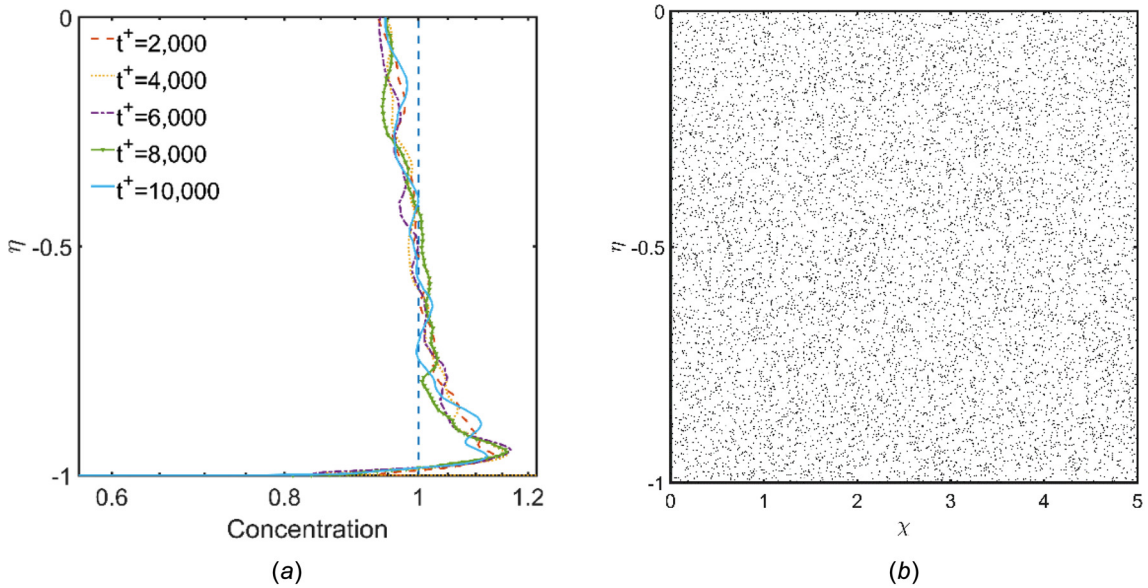

Fig. 5 (*a*) Time evolutions of fluid-tracer normalized concentration profiles and (*b*) particle distributions at 10,000 wall units

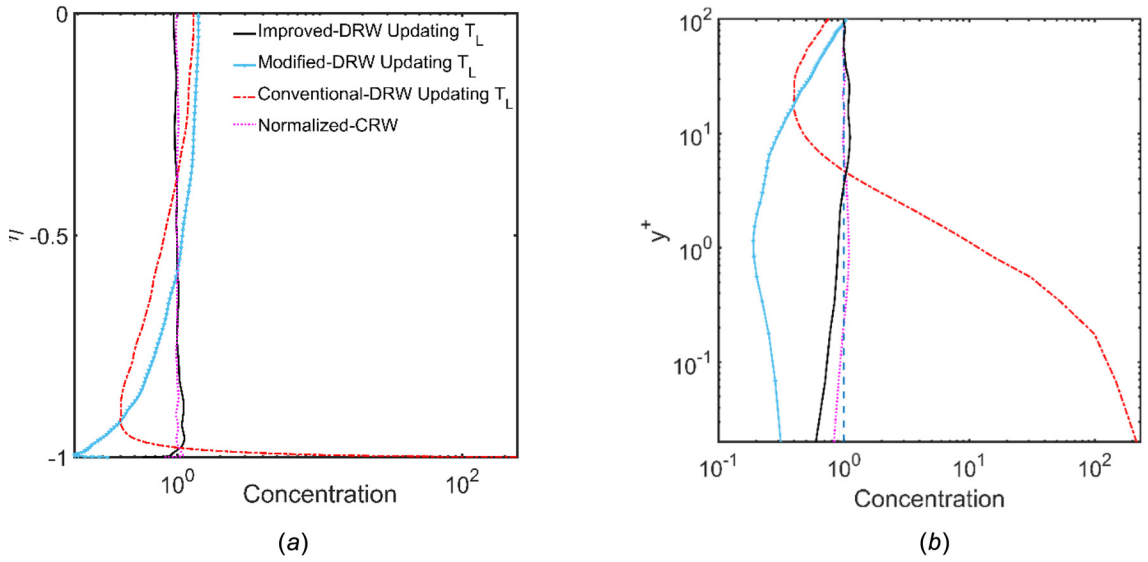

Fig. 6 The normalized concentration profiles of fluid-tracer particles predicted by the conventional-, modified-, improved-DRW, as well as the normalized-CRW models at 10,000 wall units: (*a*) linear plots along with the half-height of the channel and (*b*) log–log plots in the near-wall region

The necessity of including the finite-inertia coefficient (FIC) of $1/(1+\text{Stk})$ for the drift term of the normalized-CRW model was discussed in detail by Bocksell and Loth [39] and Mofakham and Ahmadi [19]. Based on these earlier studies, it is hypothesized that the finite-inertia coefficient also needs to be included in the drift terms of the improved-DRW model. For clarifying the effects of the FIC on the performance of the improved-DRW model, the predicted concentration profiles for finite-size particles with non-dimensional relaxation times of 0.2, 1, 5, 15, 25, and 125 for the cases with and without FIC for time and velocity gradient drift terms are explored. Table 4 describes the drift terms for different cases. Case 1 is when the FIC is included in both the velocity and time gradient drift terms. In case 2, the FIC is only included in the velocity gradient drift term, and in case 3, it is only included in the time gradient drift term. Finally, in case 4, The FIC is ignored in both the velocity and time drift terms.

A series of simulations are conducted with the reflecting boundary condition on the walls, and the normalized concentrations are

Table 4 Different cases assumed for the drift terms of the improved DRW model

	Case 1	Case 2	Case 3	Case 4
Drift terms	$\frac{1}{1+\text{Stk}}\left(\sigma_i\frac{\partial\sigma_i}{\partial x_i}dt-\sigma_i^2\frac{\partial T_L}{\partial x_i}\frac{dt}{T_L}\right)$	$\frac{1}{1+\text{Stk}}\sigma_i\frac{\partial\sigma_i}{\partial x_i}dt-\sigma_i^2\frac{\partial T_L}{\partial x_i}\frac{dt}{T_L}$	$\sigma_i\frac{\partial\sigma_i}{\partial x_i}dt-\frac{1}{1+\text{Stk}}\sigma_i^2\frac{\partial T_L}{\partial x_i}\frac{dt}{T_L}$	$\sigma_i\frac{\partial\sigma_i}{\partial x_i}dt-\sigma_i^2\frac{\partial T_L}{\partial x_i}\frac{dt}{T_L}$

calculated at 675, 1125, 2000, 4000, 6000, 8000, and 10,000 wall units, and the results at 675 and 1125, and 10,000 wall units are plotted in Fig. 7. The result at 10,000 wall units can be considered as roughly the steady-state condition.

For assessing the accuracy of these simulations, the near-wall normalized concentration predictions for different cases are compared with those of the normalized-CRW model (Eq. (28)), and the DNS data of Marchioli et al. [48] at 675 and 1125 wall units in a channel with shear Reynolds number of 150 and the reflecting boundary condition on the walls.

For exploring the discrepancies between the predictions of the improved-DRW and the DNS data, in Table 5, the RMS of the differences between the predicted concentrations (at the positions where the DNS data are available) at 675 and 1125 wall units for different particle sizes are evaluated using

$$\Delta_{\mathrm{DNS}} = \mathrm{rms}\left(\mathrm{concentration}_{\mathrm{model}} - \mathrm{concentration}_{\mathrm{DNS}}\right) \tag{32}$$

In addition, in Table 6, the RMS differences between the predictions of the improved-DRW models and those of the normalized-

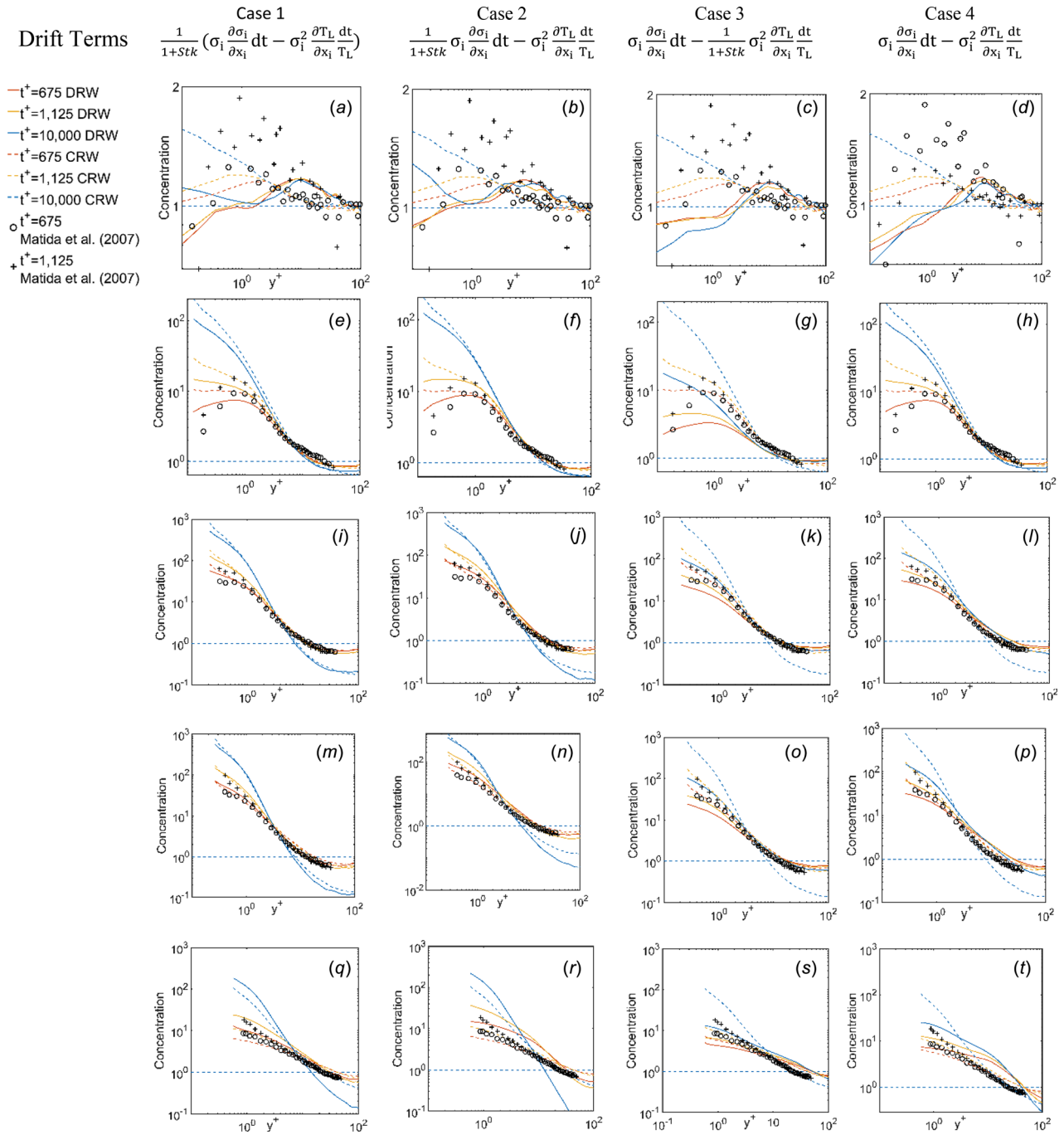

Fig. 7 Comparison of the improved-DRW model predictions of the normalized concentration including the FIC for both of the time and velocity gradient drift terms (case 1) ((*a*), (*e*), (*i*), (*m*), (*q*), and (*u*)), including the FIC only for the velocity gradient drift term (case 2) ((*b*), (*f*), (*j*), (*n*), (*r*), and (*v*)), including the FIC only for the time gradient drift term (case 3) ((*c*), (*g*), (*k*), (*o*), (*s*), and (*w*)], and ignoring the FIC for both of the drift terms (case 4) [(*d*), (*h*), (*l*), (*p*), (*t*), and (*x*)] with those of the normalized-CRW model and the DNS data of Marchioli et al. [48] with particles with relaxation time of (*a*)–(*d*) 0.2, (*e*)–(*h*) 5, (*i*)–(*l*) 15, (*m*)–(*p*) 25, and (*q*)–(*t*) 125 at different times in wall units.

Table 5 The RMS differences between the predictions of different models and the DNS data at 675 and 1125 wall units

	Improved-DRW								Normalized-CRW	
	Case 1		Case 2		Case 3		Case 4		With FIC	
τ^+	$t^+ = 675$	$t^+ = 1125$	$t^+ = 675$	$t^+ = 1125$	$t^+ = 675$	$t^+ = 1125$	$t^+ = 675$	$t^+ = 1125$	$t^+ = 675$	$t^+ = 1125$
0.2	0.33	0.10	0.32	0.09	0.34	0.12	0.36	0.12	0.29	0.06
1	0.28	0.42	0.25	0.37	0.44	0.60	0.41	0.58	0.22	0.32
5	0.95	2.27	1.04	2.39	2.14	3.52	1.82	3.06	1.78	4.36
15	3.70	8.67	7.88	16.80	4.83	9.99	2.83	6.22	5.62	13.61
25	4.28	6.72	9.77	17.01	6.00	14.77	3.26	9.97	2.36	4.92
125	1.01	2.03	3.03	5.96	1.49	3.33	1.26	2.31	0.93	2.27

CRW model at 10,000 wall units for different particle sizes are evaluated using

$$\Delta_{\mathrm{CRW}} = \mathrm{rms}\left(\mathrm{concentration}_{\mathrm{DRW\,model}} - \mathrm{concentration}_{\mathrm{CRW}}\right) \quad (33)$$

Figure 7(*a*) shows that for case 1 where the FIC are included for both velocity and time gradient terms, the concentration predictions for $\tau^+ = 0.2$ oscillate around a concentration of one. Although the new model slightly underestimates the concentration of particles for y^+ less than 10 in comparison to the DNS data and the normalized-CRW predictions, the small differences reported in Tables 5 and 6 confirm the reasonable agreement between the results. Figures 7(*b*)–7(*d*) show that ignoring the FIC for the time gradient and/or for the velocity gradient terms does not significantly affect the results for particles with a nondimensional relaxation time of 0.2. The small variation of the RMS difference values listed in Tables 5 and 6 also confirms this conclusion.

By comparing the results illustrated in Figs. 7(*e*)–7(*h*), it is found that case 1 predicts a slightly smaller concentration for particles with a relaxation time of 5 in the near-wall region in comparison to the DNS data and those of the CRW model. For this size particle, the predictions of case 2 are in a slightly better agreement with those of the CRW model and the DNS data. However, the concentration profiles predicted by case 3 and 4 are significantly underestimated. Tables 5 and 6 also show that the errors for cases 1 and 2 are almost identical for $\tau^+ = 5$, but larger errors are seen for cases 3 and 4.

As it is shown in Fig. 7(*i*), the predictions of the improved-DRW Modal (case 1) for $\tau^+ = 15$ are in an excellent agreement with those of the CRW model and the DNS data. Ignoring the FIC for the time drift term (Fig. 7(*j*)) leads to the overestimation of the particle concentration at around 1 wall units away from the wall. Ignoring the FIC for the velocity gradient term (Figs. 7(*k*) and 7(*l*)), however, markedly reduces the concentration of particles in the near-wall region and increases the discrepancies between the DRW predictions and the DNS data and those of the CRW model as it is shown in Figs. 7(*i*)–7(*l*). The corresponding errors reported in Table 5 for $\tau^+ = 15$ also confirm that the predictions of case 1 are in a better agreement with the DNS data in comparison to those of cases 2–4. In addition, Table 6 shows that the differences evaluated for cases 1 and 2 are comparable, while much larger errors are found for cases 3 and 4.

Table 6 The RMS differences between the predictions of the cases whose drift terms are listed in Table 4 and those of the normalized-CRW model at 10,000 wall units

τ^+	Case 1	Case 2	Case 3	Case 4
0.2	0.11	0.10	0.19	0.18
1	0.43	0.44	0.73	0.75
5	11.68	28.16	24.93	24.14
15	35.47	15.38	94.21	88.28
25	26.52	21.88	91.01	83.78
125	16.01	22.09	16.20	13.49

Figure 7(*m*) also illustrates that the predictions of the improved-DRW modal (case 1) for $\tau^+ = 25$ are in a good agreement with those of the CRW model and the DNS data, but ignoring the FIC for the time gradient drift term in case 2 (Fig. 7(*n*)) and ignoring the FIC for the velocity gradient drift term in case 3 (Fig. 7(*o*)), respectively, leads to the overestimation and underestimation of the near-wall DNS data and the CRW predictions. The effects of ignoring the FIC for both the time and velocity gradient drift terms (case 4) are shown in Fig. 7(*p*). It is seen that the concentration profiles of this case are slightly larger than those of case 3. The RMS differences listed in Table 5 clearly show that case 1 has the closest agreement with the DNS data. The discrepancies between the DRW and the CRW predictions listed in Table 6 for $\tau^+ = 15$ show that the predictions of case 2 are in a slightly better agreement with those of the CRW model at 10,000 wall units, but the differences for cases 3 and 4 are markedly larger.

Figures 7(*q*)–7(*t*) show that the predictions of case 1 for $\tau^+ = 125$ has the best agreement with the CRW model and the DNS data. In addition, the average errors evaluated in Table 5 confirm the exceptional performance of case 1 compared to other models (cases 2–4). While smaller errors are seen for case 4 in Table 6, Fig. 7(*t*) clarifies that this case does not correctly estimate the trend for the near-wall concentration variations.

3.4 Finite-Size Particles. In this section, the accuracy of different DRW models in predicting the concentration profiles and deposition velocities for a wide range of micro- and nanoparticles with assuming the trap boundary condition on the walls are explored.

3.4.1 Concentration Profiles. In Fig. 8, the steady-state normalized concentration profiles of different sizes of particles predicted by the conventional-, modified-, and improved-DRW models are shown.

It is well known that particles with large inertia accumulate in the near-wall regions as a result of the turbophoresis effects [49,50]. Accordingly, as it is seen in Fig. 8(*a*), all versions of the DRW model, as well as the normalized-CRW model, predict a buildup of 30 μm particle concentration in the near-wall region. The figure indicates that the predictions of the conventional- and modified-DRW models are roughly identical with a maximum normalized concentration of around 10 in the near-wall region. In contrast, the improved-DRW and the CRW model, respectively, predicts a maximum concentration of 14.4 and 6.5. The higher near-wall concentration prediction of the improved-DRW model compared to that of the normalized-CRW model can be traced to the smaller deposition velocity of 30 μm particles predicted by the improved-DRW model. This point is further discussed in Sec. 3.4.2.

The comparison of the DRW and CRW predictions of 10 μm particle concentrations shown in Fig. 8(*b*) indicates that the conventional-DRW estimates the normalized concentration of 49

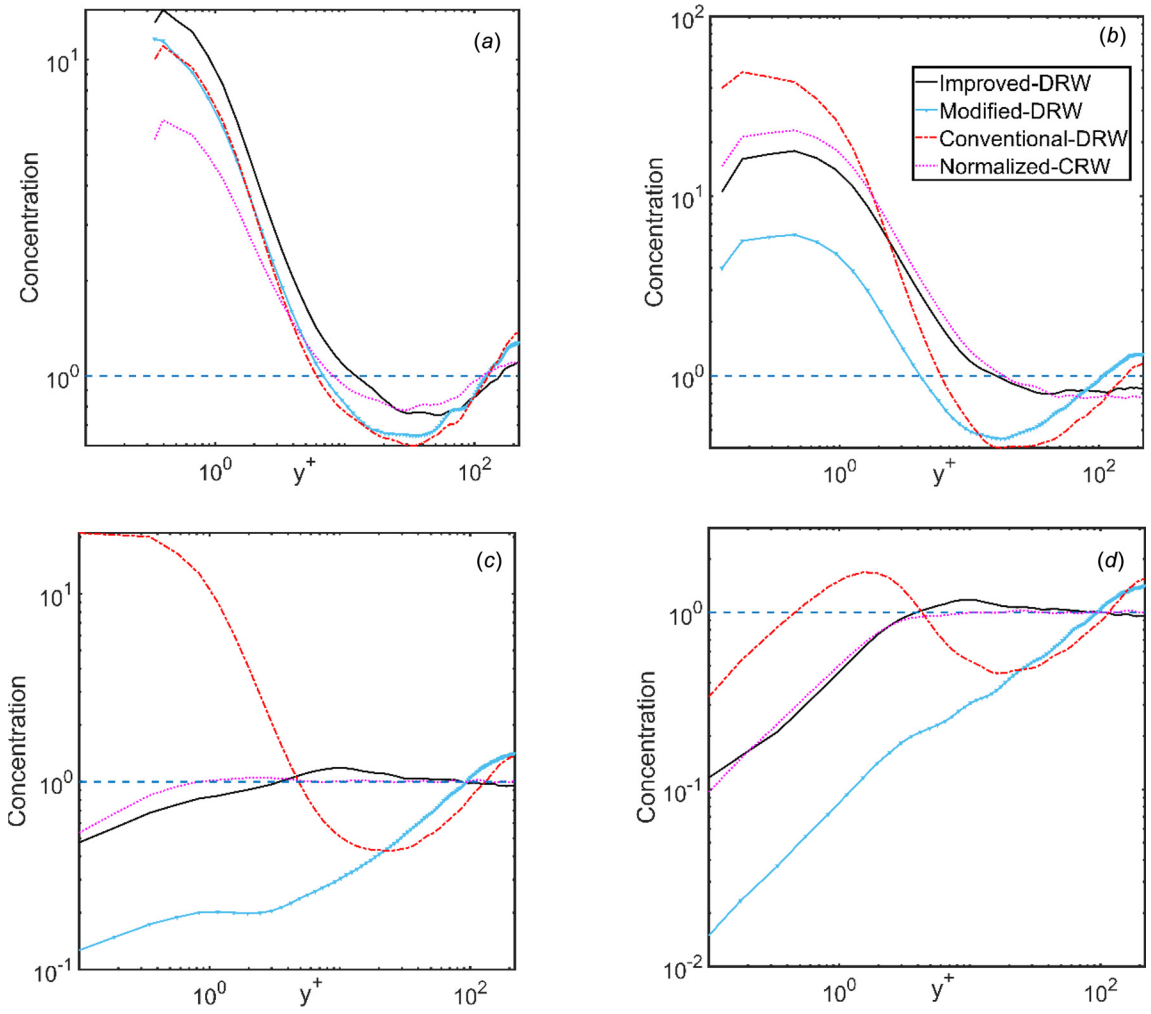

Fig. 8 Comparison between the normalized concentration profiles predicted by the conventional-, modified-, and improved-DRW models for particles with diameters of (*a*) 30 μm, (*b*) 10 μm, (*c*) 1 μm, and (*d*) 10 nm

for the near-wall accumulations, while the modified-DRW model estimates a concertation profile with a maximum value of around 6 and the improved-DRW model predicts a maximum concentration of around 17.4. From this comparison, it is seen that the conventional- and modified-DRW models, respectively, overestimates and underestimates the accumulation of 10 μm in the near-wall region compared to the normalized-CRW model. However, the prediction of the improved-DRW model is close to that of the normalized-CRW model for the normalized concentration of about 22.5.

The concentration estimations of 1 μm particles are shown in Fig. 8(*c*). Since particles with a diameter equal to less than 1 μm almost follow fluid particle trajectories, it is expected to get uniform particle distributions with no near-wall accumulation of particles. However, Fig. 8(*c*) indicates that the conventional-DRW model estimates a maximum concentration of 20.6 for the near-wall region. Using the modified-DRW model remarkably reduces the near-wall accumulation of 1 μm particles, but this model leads to a concentration profile with values less than one in the near-wall region and larger than one in the core region. However, using the improved-DRW model results in an almost uniform concentration profile, which is also in good agreement with the prediction of the CRW model with no near-wall accumulation.

The estimations of the DRW and CRW models for the concentration of 10 nm particles are illustrated in Fig. 8(*d*). The concentration predictions of the conventional- and modified-DRW models for these ultrafine particles are not uniform. However, the improved-DRW model estimates uniform distributions, which is in good agreement with those of the normalized-CRW model.

3.4.2 Deposition Velocities. In Fig. 9, the deposition velocities of 10 nm to 30 μm particles predicted by the conventional-, modified-, and improved-DRW models are plotted versus the non-dimensional particle relaxation time τ^+. To assess the accuracy of these results, they are compared with the experimental data collected by Papavergos and Hedley [51], earlier numerical results [19,25,52–55], the DNS data [41,48,56], and the predictions of the empirical models [34,35,57]. This figure shows that the available experimental data for deposition velocity for particles with $\tau^+ > 0.1$ are scattered (in part due to direction of gravity for upward, downward flows). This makes it hard to identify the best model for prediction of deposition velocities of large size particles. However, for Brownian particles $\tau^+ < 0.1$, the empirical model of Fan and Ahmadi [34] which was based on a theoretical diffusion model, and also matches with the empirical model of Wood [35] provides in a more precise criteria for identifying the model with the best performance.

It is worth mentioning that the deposition velocities of the modified- and improved-DRW models for particles with diameters between 500 nm and 50 μm ($0.004 < \tau^+ < 3.5$) with small deposition rates were evaluated with 1×10^6 particles to reduce the statistical error.

It is seen that the conventional-DRW overestimates the deposition velocities up to three orders of magnitude due to the

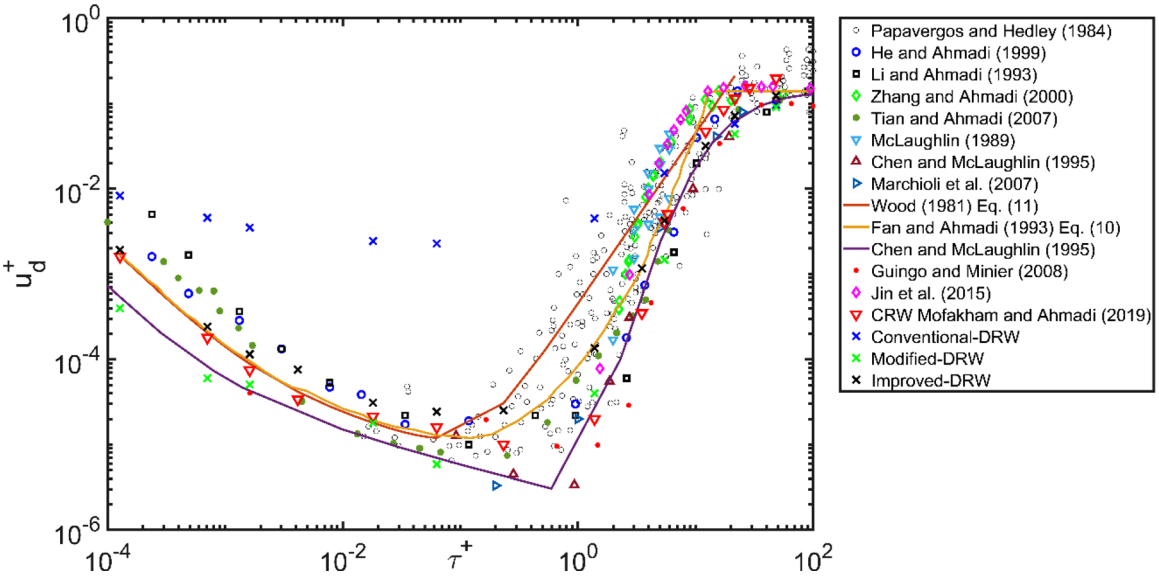

Fig. 9 Comparison of the nondimensional deposition velocities predicted by the conventional-, modified-, and improved-DRW models with the experimental data, empirical results, and the earlier numerical estimations

overestimation of the near-wall particle concentration, as discussed in Sec. 3.4.1. By including the velocity gradient drift term in the modified-DRW model, the predictions of deposition velocities are dramatically improved. However, the corresponding deposition rates are underestimated as a result of the depletion of particles from the near-wall regions, as discussed in Sec. 3.4.1.

Figure 9 shows that the predictions of the improved-DRW model for deposition velocities in the diffusion regime ($\tau^+ < 1$) [58] are almost identical to those of the normalized-CRW model and the empirical models, which were based on the theoretical diffusion approach. For the inertia-impaction regime [35,58] for which the uncertainties of the available data are around two orders of magnitudes [48,56], the predictions of the improved-DRW model are in good agreement with the experimental data. The improved-DRW model, however, slightly overestimates and underestimate the normalized-CRW results, respectively, for $\tau^+ < 10$ and $\tau^+ > 10$. The smaller deposition velocity predicted by the improved-DRW model for large size particles (30 μm) results in larger accumulation of particles in the near-wall region as was noted in the discussion of Fig. 8(*a*).

4 Conclusions

The performance of the conventional-DRW model, Eq. (24), in inhomogeneous turbulent flows was explored. It was shown that the inhomogeneities of the turbulence fluctuating velocity and Lagrangian time scales adversely affect the performance of the DRW model leading to inaccurate concentration profiles and deposition velocities. To improve the performance of the DRW model, the suggested drift term in the literature, which is a function of the gradient of the RMS velocity fluctuations, was included in the modified-DRW model using Eqs. (25) and (26). It was found that the predicted concentration profiles of tracer particles predicted by the modified-DRW are still nonuniform. It was hypothesized that the reason for this erroneous prediction is due to the inhomogeneous turbulence time macroscale in the channel flow. A new drift correction term as a function of gradients of both RMS fluctuation velocity and the turbulence time macroscale as given by Eq. (27) was proposed. It was shown that the new improved-DRW model performs properly in inhomogeneous turbulent flows.

From the presented simulations, the following conclusions are drawn:

- Ignoring the turbulence velocity gradient drift term leads to the accumulation of fluid-tracer particles in regions with low turbulence intensities near walls. However, ignoring the Lagrangian time gradient drift term results in the migration of fluid-tracer particles to regions with relatively large turbulence time scale (core region).
- For obtaining uniform concentration profiles for fluid-tracer and submicron particles and accurate concentration profiles for large size particles, it is essential to include both the gradients of turbulence Lagrangian time in addition to the RMS velocity in the drift term of the DRW model.
- Errors in the predictions of the concentration profiles result in the corresponding inaccurate particle deposition velocities.
- It is critical to include the finite-inertial coefficient (FIC) for the drift correction terms to incorporate the turbophoresis effects to accurately predict the accumulation of large size particles in the near-wall regions.
- For large size particles with large Stokes numbers, the discrepancies between the predictions of the conventional-, modified-, and improved-DRW models are less significant due to the use of the finite-inertial coefficient. A series of performed simulations (the results were not reported for the sake of brevity), the predictions of the conventional-DRW model become similar to those of the improved-DRW model for particles larger than 100 μm for the range of flow velocities considered in this study.
- In general, using the conventional-DRW model in inhomogeneous flows results in depletions of different size particles from regions with high turbulence intensities to regions with small turbulence intensities, which is not realistic for small size particles. Since generally near-wall regions have the smallest turbulence intensities, particles tend to accumulate in near-wall regions independent of the passage geometry, which results in an overestimation of the corresponding (small size) particle deposition velocities.
- The use of modified-DRW model in inhomogeneous flows results in migration of particles to regions with larger turbulence time scales so that the concentration of particles in the near-wall regions with small turbulence time scale are reduced which leads the underestimations of particle deposition on walls.
- The concentration profiles and deposition velocities resulting from the improved-DRW model are roughly identical to

those of the normalized-CRW model, while the normalized-CRW does not need the time gradient drift term, predicts more uniform concentration profiles for submicron particles, and somewhat more accurate deposition velocities.

While the present study was focused on channel flows, the developed stochastic models for simulating turbulence fluctuation should be applicable to more complex flow configuration. Application of the improved-DRW to three-dimensional turbulent flows is under investigation and results will be reported in the future.

Acknowledgment

The first author, Amir A. Mofakham, was the Hill Graduate Student Fellow at Clarkson University during the course of his Ph.D. study. He also was the recipient of the ASME Fluids Engineering Division Graduate Student Scholarship in 2019 and 2020 for this research.

Nomenclature

Overbar signifies mean value

C_c = Stokes Cunningham slip correction factor
C_D = particle drag coefficient
D = particle mass diffusivity
d_p = particle diameter
d_p^+ = nondimensional particle diameter
f = elliptic relaxation function
G_i = vector Gaussian random number with zero mean and unit variance
H^+ = nondimensional channel half-width
k = turbulence kinetic energy
k_b = Boltzmann constant
k^+ = nondimensional turbulence kinetic energy
L_t = turbulence length scale
L^+ = nondimensional channel length
m = particle mass
N_p = number of deposited particles
N_0 = total number of particles
P_k = turbulence production kinetic energy
$\mathrm{Re_p}$ = particle Reynolds number
S = particle to fluid density ratio
S_0 = spectral intensity of the Brownian noise
Sc = Schmidt number
Stk = Stokes number
t = time
T = absolute temperature
t_{int} = interaction time scale
T_L = Lagrangian integral time scale
T_t = Eulerian turbulent time scale
t_d^+ = nondimensional time interval
T_L^+ = nondimensional Lagrangian integral time scale
$\mathbf{u}$ = fluid velocity vector
$\mathbf{u}^*$ = shear velocity
u_{i}, u_j = fluid velocity components
u_{p} = particle velocity vector
u_{i}' = fluid fluctuating velocity components seen by particles
$\overline{u_i'^{\mathrm{n+1}}}$ = mean drift velocity
u_{i}^p = particle velocity components
u_d^+ = nondimensional deposition velocity
$\overline{v'^2}$ = variance wall-normal fluid velocity fluctuation
x_i, x_j = position vector components
y^+ = nondimensional wall distance
ε = dissipation rate
λ = gas mean free path
μ = particle fluid viscosity
ξ_{i} = vector Gaussian random number
σ_i = RMS velocity fluctuations component
τ_w = wall shear stress
τ_p = particle relaxation time
τ_p^+ = nondimensional particle relaxation time
ν = kinematic viscosity
ν_t = eddy viscosity

References

[1] Davudov, D., Moghanloo, R. G., and Flom, J., 2018, "Scaling Analysis and Its Implication for Asphaltene Deposition in a Wellbore," SPE J., **23**(02), pp. 274–285.
[2] Luo, K., Yu, H., Dai, Z., Fang, M., and Fan, J., 2016, "CFD Simulations of Flow and Dust Dispersion in a Realistic Urban Area," Eng. Appl. Comput. Fluid Mech., **10**(1), pp. 228–242.
[3] Chalupa, D. C., Morrow, P. E., Oberdörster, G., Utell, M. J., and Frampton, M. W., 2004, "Ultrafine Particle Deposition in Subjects With Asthma," Environ. Health Perspectives, **112**(8), pp. 879–882.
[4] Tian, L., and Ahmadi, G., 2012, "Transport and Deposition of Micro-and Nano-Particles in Human Tracheobronchial Tree by an Asymmetric Multi-Level Bifurcation Model," J. Comput. Multiphase Flows, **4**(2), pp. 159–182.
[5] Tian, L., and Ahmadi, G., 2013, "Fiber Transport and Deposition in Human Upper Tracheobronchial Airways," J. Aerosol Sci., **60**, pp. 1–20.
[6] Tavakol, M. M., Ghahramani, E., Abouali, O., Yaghoubi, M., and Ahmadi, G., 2017, "Deposition Fraction of Ellipsoidal Fibers in a Model of Human Nasal Cavity for Laminar and Turbulent Flows," J. Aerosol Sci., **113**, pp. 52–70.
[7] Finlay, W. H., 2019, "Aerosol Physics and Lung Deposition Modeling," *Pharmaceutical Inhalation Aerosol Technology*, Taylor and Francis Group, Boca Raton, FL, p. 81.
[8] Innocenti, A., Marchioli, C., and Chibbaro, S., 2016, "Lagrangian Filtered Density Function for LES-Based Stochastic Modelling of Turbulent Particle-Laden Flows," Phys. Fluids, **28**(11), p. 115106.
[9] Marchioli, C., 2017, "Large-Eddy Simulation of Turbulent Dispersed Flows: A Review of Modelling Approaches," Acta Mech., **228**(3), pp. 741–771.
[10] Taylor, G. I., 1922, "Diffusion by Continuous Movements," Proc. London Math. Soc., **s2-20**(1), pp. 196–212.
[11] Gosman, A. D., and Loannides, E., 1983, "Aspects of Computer Simulation of Liquid-Fueled Combustors," J. Energy, **7**(6), pp. 482–490.
[12] Legg, B. J., and Raupach, M. R., 1982, "Markov-Chain Simulation of Particle Dispersion in Inhomogeneous Flows: The Mean Drift Velocity Induced by a Gradient in Eulerian Velocity Variance," Boundary-Layer Meteorol., **24**(1), pp. 3–13.
[13] MacInnes, J. M., and Bracco, F. V., 1992, "Stochastic Particle Dispersion Modeling and the Tracer-Particle Limit," Phys. Fluids A: Fluid Dyn., **4**(12), pp. 2809–2824.
[14] Iliopoulos, I., and Hanratty, T. J., 1999, "Turbulent Dispersion in a Non-Homogeneous Field," J. Fluid Mech., **392**, pp. 45–71.
[15] Bocksell, T. L., and Loth, E., 2001, "Random Walk Models for Particle Diffusion in Free-Shear Flows," AIAA J., **39**(6), pp. 1086–1096.
[16] Mito, Y., and Hanratty, T. J., 2002, "Use of a Modified Langevin Equation to Describe Turbulent Dispersion of Fluid Particles in a Channel Flow," Flow, Turbul. Combust., **68**(1), pp. 1–26.
[17] Jayaraju, S. T., Sathiah, P., Roelofs, F., and Dehbi, A., 2015, "RANS Modeling for Particle Transport and Deposition in Turbulent Duct Flows: Near Wall Model Uncertainties," Nucl. Eng. Des., **289**, pp. 60–72.
[18] Mofakham, A. A., and Ahmadi, G., 2019, "Accuracy of the CRW Models for Prediction of the Deposition and Dispersion of Particles in Inhomogeneous Turbulent Channel Flows," ASME Paper No. AJKFluids2019-4856.
[19] Mofakham, A. A., and Ahmadi, G., 2019, "Particles Dispersion and Deposition in Inhomogeneous Turbulent Flows Using Continuous Random Walk Models," Phys. Fluids, **31**(8), p. 083301.
[20] Mofakham, A. A., and Ahmadi, G., 2020, "On Random Walk Models for Simulation of Particle-Laden Turbulent Flows," Int. J. Multiphase Flow, **122**, p. 103157.
[21] Monin, A. S., and Yaglom, A. M., 1973, *Statistical Fluid Mechanics: Mechanics of Turbulence*, **1**, MIT Press, Cambridge, Mass English ed. updated, Augmented and Rev.
[22] Durbin, P. A., 1980, "A Random Flight Model of Inhomogeneous Turbulent Dispersion," Phys. Fluids, **23**(11), p. 2151.
[23] Durbin, P. A., 1983, "Stochastic Differential Equations and Turbulent Dispersion," NASA Lewis Research Center, Cleveland, OH, Report No. NASA RP 1103c.1.
[24] Durbin, P. A., 1984, "Comments on Papers by Wilson et al.(1981) and Legg and Raupach (1982)," Boundary-Layer Meteorol., **29**(4), pp. 409–411.
[25] Tian, L., and Ahmadi, G., 2007, "Particle Deposition in Turbulent Duct Flows—Comparisons of Different Model Predictions," J. Aerosol Sci., **38**(4), pp. 377–397.
[26] Durbin, P. A., 1991, "Near-Wall Turbulence Closure Modeling Without 'Damping Functions," **3**(1), p. 13.
[27] Durbin, P. A., 1993, "Application of a Near-Wall Turbulence Model to Boundary Layers and Heat Transfer," Int. J. Heat Fluid Flow, **14**(4), pp. 316–323.
[28] Lien, F.-S., and Kalitzin, G., 2001, "Computations of Transonic Flow With the v^2–f Turbulence Model," Int. J. Heat Fluid Flow, **22**(1), pp. 53–61.
[29] Davidson, L., 2003, "Modification of the V^2f Model for Computing the Flow in a 3D Wall Jet," Turbul. Heat Mass Trans., **4**, pp. 577–584.
[30] Ounis, H., Ahmadi, G., and McLaughlin, J. B., 1991, "Brownian Diffusion of Submicrometer Particles in the Viscous Sublayer," J. Colloid Interface Sci., **143**(1), pp. 266–277.

[31] Li, A., and Ahmadi, G., 1993, "Deposition of Aerosols on Surfaces in a Turbulent Channel Flow," Int. J. Eng. Sci., **31**(3), pp. 435–451.
[32] Matida, E. A., Nishino, K., and Torii, K., 2000, "Statistical Simulation of Particle Deposition on the Wall From Turbulent Dispersed Pipe Flow," Int. J. Heat Fluid Flow, **21**(4), pp. 389–402.
[33] Hinds, W. C., 1999, *Aerosol Technology: Properties, Behavior, and Measurement of Airborne Particles*, John Wiley & Sons, Hoboken, NJ.
[34] Fan, F.-G., and Ahmadi, G., 1993, "A Sublayer Model for Turbulent Deposition of Particles in Vertical Ducts With Smooth and Rough Surfaces," J. Aerosol Sci., **24**(1), pp. 45–64.
[35] Wood, N. B., 1981, "A Simple Method for the Calculation of Turbulent Deposition to Smooth and Rough Surfaces," J. Aerosol Sci., **12**(3), pp. 275–290.
[36] Majlesara, M., Salmanzadeh, M., and Ahmadi, G., 2013, "A Model for Particles Deposition in Turbulent Inclined Channels," J. Aerosol Sci., **64**, pp. 37–47.
[37] Brown, D. J., and Hutchinson, P., 1979, "The Interaction of Solid or Liquid Particles and Turbulent Fluid Flow Fields—A Numerical Simulation," ASME J. Fluids Eng., **101**(2), pp. 265–269.
[38] Kallio, G. A., and Reeks, M. W., 1989, "A Numerical Simulation of Particle Deposition in Turbulent Boundary Layers," Int. J. Multiphase Flow, **15**(3), pp. 433–446.
[39] Bocksell, T. L., and Loth, E., 2006, "Stochastic Modeling of Particle Diffusion in a Turbulent Boundary Layer," Int. J. Multiphase Flow, **32**(10–11), pp. 1234–1253.
[40] Iliopoulos, I., and Hanratty, T. J., 2004, "A Non-Gaussian Stochastic Model to Describe Passive Tracer Dispersion and Its Comparison to a Direct Numerical Simulation," Phys. Fluids, **16**(8), pp. 3006–3030.
[41] McLaughlin, J. B., 1989, "Aerosol Particle Deposition in Numerically Simulated Channel Flow," Phys. Fluids A: Fluid Dyn., **1**(7), pp. 1211–1224.
[42] Ounis, H., Ahmadi, G., and McLaughlin, J. B., 1993, "Brownian Particle Deposition in a Directly Simulated Turbulent Channel Flow," Phys. Fluids A: Fluid Dyn., **5**(6), pp. 1427–1432.
[43] Nasr, H., Ahmadi, G., and Mclaughlin, J. B., 2009, "A DNS Study of Effects of Particle–Particle Collisions and Two-Way Coupling on Particle Deposition and Phasic Fluctuations," J. Fluid Mech., **640**, pp. 507–536.
[44] Mofakham, A. A., Ahmadi, G., and McLaughlin, J., 2018, "Interactions of Flow Structure With Nano- and Micro-Particles in Turbulent Channel Flows," ASME Paper No. FEDSM2018-83349.
[45] Kim, J., Moin, P., and Moser, R., 1987, "Turbulence Statistics in Fully Developed Channel Flow at Low Reynolds Number," J. Fluid Mech., **177**, pp. 133–166.
[46] Moser, R. D., Kim, J., and Mansour, N. N., 1999, "Direct Numerical Simulation of Turbulent Channel Flow Up to Re T = 590," Phys. Fluids, **11**(4), pp. 943–945.
[47] Mansour, N. N., Kim, J., and Moin, P., 1988, "Reynolds-Stress and Dissipation-Rate Budgets in a Turbulent Channel Flow," J. Fluid Mech., **194**(1), p. 15.
[48] Marchioli, C., Picciotto, M., and Soldati, A., 2007, "Influence of Gravity and Lift on Particle Velocity Statistics and Transfer Rates in Turbulent Vertical Channel Flow," Int. J. Multiphase Flow, **33**(3), pp. 227–251.
[49] Caporaloni, M., Tampieri, F., Trombetti, F., and Vittori, O., 1975, "Transfer of Particles in Nonisotropic Air Turbulence," J. Atmos. Sci., **32**(3), pp. 565–568.
[50] Reeks, M. W., 1983, "The Transport of Discrete Particles in Inhomogeneous Turbulence," J. Aerosol Sci., **14**(6), pp. 729–739.
[51] Papavergos, P. G., and Hedley, A. B., 1984, "Particle Deposition Behaviour From Turbulent Flows," Chem. Eng. Res. Des., **62**(5), pp. 275–295.
[52] Li, A., and Ahmadi, G., 1992, "Dispersion and Deposition of Spherical Particles From Point Sources in a Turbulent Channel Flow," Aerosol Sci. Technol., **16**(4), pp. 209–226.
[53] He, C., and Ahmadi, G., 1999, "Particle Deposition in a Nearly Developed Turbulent Duct Flow With Electrophoresis," J. Aerosol Sci., **30**(6), pp. 739–758.
[54] Guingo, M., and Minier, J.-P., 2008, "A Stochastic Model of Coherent Structures for Particle Deposition in Turbulent Flows," Phys. Fluids, **20**(5), p. 053303.
[55] Jin, C., Potts, I., and Reeks, M. W., 2015, "A Simple Stochastic Quadrant Model for the Transport and Deposition of Particles in Turbulent Boundary Layers," Phys. Fluids, **27**(5), p. 053305.
[56] Zhang, H., and Ahmadi, G., 2000, "Aerosol Particle Transport and Deposition in Vertical and Horizontal Turbulent Duct Flows," J. Fluid Mech., **406**, pp. 55–80.
[57] Chen, M., and McLaughlin, J. B., 1995, "A New Correlation for the Aerosol Deposition Rate in Vertical Ducts," J. Colloid Interface Sci., **169**(2), pp. 437–455.
[58] Young, J., and Leeming, A., 1997, "A Theory of Particle Deposition in Turbulent Pipe Flow," J. Fluid Mech., **340**, pp. 129–159.